AIP | Applied Physics Letters

Biomedical terahertz imaging with a quantum cascade laser

Seongsin M. Kim, Fariba Hatami, James S. Harris, Allison W. Kurian, James Ford et al.

Citation: Appl. Phys. Lett. **88**, 153903 (2006); doi: 10.1063/1.2194229
View online: http://dx.doi.org/10.1063/1.2194229
View Table of Contents: http://apl.aip.org/resource/1/APPLAB/v88/i15
Published by the American Institute of Physics.

Biomedical terahertz imaging with a quantum cascade laser

Seongsin M. Kim,[a] Fariba Hatami, and James S. Harris
Solid State Photonics Laboratory, Stanford University, Stanford, California 94305

Allison W. Kurian and James Ford
School of Medicine, Division of Oncology, Stanford University, Stanford, California 94305

Douglas King
Hansen Experimental Physics Laboratory, Stanford University, Stanford, California 94305

Giacomo Scalari, Marcella Giovannini, Nicolas Hoyler, and Jerome Faist
Institute of Physics, University of Neuchâtel, Neuchâtel CH-2000, Switzerland

Geoff Harris
University of California, Davis Medical Center, Sacramento, California 95817

(Received 18 November 2005; accepted 1 March 2006; published online 14 April 2006)

We present biomedical imaging using a single frequency terahertz imaging system based on a low threshold quantum cascade laser emitting at 3.7 THz ($\lambda = 81\ \mu$m). With a peak output power of 4 mW, coherent terahertz radiation and detection provide a relatively large dynamic range and high spatial resolution. We study image contrast based on water/fat content ratios in different tissues. Terahertz transmission imaging demonstrates a distinct anatomy in a rat brain slice. We also demonstrate malignant tissue contrast in an image of a mouse liver with developed tumors, indicating potential use of terahertz imaging for probing cancerous tissues. © *2006 American Institute of Physics*. [DOI: 10.1063/1.2194229]

Since Hu and Nuss showed the first imaging in the frequency range between 0.1 and 2.0 THz,[1] the development of terahertz technology has focused on the 0.3–10 THz frequency gap between photonics and electronics and initial demonstrations have generated tremendous interest in the fields of sensing and imaging. Although there have been successes in demonstrating the feasibility of biochemical sensing using either terahertz time-domain spectroscopy[2–4] or continuous wave (cw) terahertz radiation based on the photomixing,[5,6] its potential for medical applications is only beginning to be explored. Because of its low interference and nonionizing characteristics, terehertz imaging is expected to be a powerful technique for safe, *in vivo* medical imaging (e.g., wound healing assessment and cancer progression tracking) and detailed imaging of soft tissues. A few research groups have demonstrated pioneering work in this field.[3,7,8] The demonstration of caries and skin cancer detection,[9,10] and comparison of malignant and normal biological tissue imaging have been reported.[11–13]

These early successes were made possible using terahertz pulsed imaging (TPI) and cw terahertz imaging. While time-domain TPI has the advantage of providing a broad frequency spectrum, it is based on picosecond terahertz pulses which require an expensive femtosecond laser and also has problems in generating narrow linewidth spectral data. By contrast, the cw terahertz imaging technique is more attractive for coherent detection with higher dynamic range of the signal to noise ratio due to its higher power spectral density. However, the current approaches for generation of cw terahertz radiation have been based on photomixing using a photoconductive antenna, which very severely limits the output power to $\sim 1\ \mu$W at frequencies above 1 THz. Recent technological advances in the area of quantum cascade lasers (QCLs) have made possible the application of QCLs for the generation of terahertz radiation[14] over a range of useful frequencies.[15,16] The potential compact and cost effective system based on high power QCLs will bring a great advantage in medical imaging over TPI and photomixing technology. QCL can also have an additional benefit to use such a frequency beyond either technique can generate without losing the merit of coherent detection. There are still challenges for QCLs to reach higher operating temperatures,[16] nevertheless, milliwatt peak terahertz powers can already be very useful for medical imaging and other applications. However, very few groups have demonstrated biomedical imaging using QC lasers.[17]

In this letter, we report biomedical imaging using a terahertz quantum cascade laser operating at 3.7 THz ($\lambda = 81\ \mu$m). We achieved a large dynamic range and high spatial resolution in the transmission imaging mode.

The terahertz quantum cascade laser used in this experiment is based on a bound-to-continuum intersubband transition design in a GaAs/AlGaAs heterostructure grown by molecular beam epitaxy. Details of the growth and fabrication have been published elsewhere.[18] The structure consists of 120 periods of active region [widths of 16.5 (2.4), 21.1 (2.7), 10.5 (1.7), 12.7 (1.3), 15.2 (1.), 18.3 (0.7), and 10 (4.2) nm ($Al_{0.15}Ga_{0.85}As$ layers are in parentheses)], embedded in a single plasmon waveguide. The laser was mounted on the cold finger of an open-flow helium cryostat. Specially designed 2 mm thick polypropylene windows were used for the cryostat, as they exhibit ~90% transmission at the laser wavelength and work as a hyperboloidal lens. The threshold current density for the laser is 0.16 kA/cm^2 and the laser emission is at a frequency of 3.7 THz ($\sim 81\ \mu$m).

Figure 1 shows the schematic diagram of the terahertz imaging system in which the laser beam is tightly focused.

[a]Author to whom correspondence should be addressed; electronic mail: seongsin@snow.stanford.edu

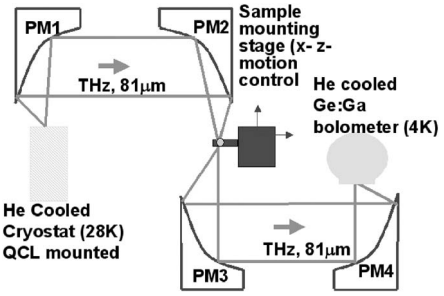

FIG. 1. Schematic diagram of terahertz imaging system using a quantum cascade laser at 3.7 THz.

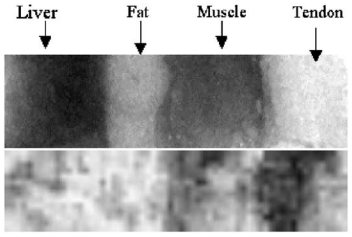

FIG. 2. Optical (photograph) image (a) and terahertz image (b) of the sample prepared from freshly cut liver, fat, muscle, and tendon. For the terahertz image the lowest transmission is indicated by black and highest transmission by white.

It consists of four off-axis parabolic mirrors. An off-axis parabolic mirror (PM1) collects the emission from the terahertz-QC laser, which is then focused and transmitted through the polypropylene hyperboloidal window. The laser beam divergence angle is about 25° and we use a 7.5 cm diameter off-axis mirror to minimize loss. The collimated terahertz radiation is then focused by PM2 to the point where the sample is mounted. The focal length of PM2 is 10 cm. The sample is mounted on a computer controlled x-y translational stage and moves in the plane perpendicular to the optic axis. We designed the sample holder so that it is transparent to the laser beam and tissues can be safely fixed on it. The terahertz beam transmitted through the sample is collimated again by a PM3 which is then refocused by PM4 onto a helium cooled germanium bolometer. The focal length of PM4 is 10 cm. The terahertz-QC laser is operated under pulse mode at 28 K. A pulse width of 300 ns and a repetition rate of 1 kHz are chosen after considering the frequency response of the Ge bolometer. The peak output power of the laser is 4 mW, which converts to a pulse energy of about 1.2 nJ.

The fundamental mode of the laser is TM ($n=1$), although the shape of the terahertz beam is expected to be elliptical, considering the geometry of the edge emitting laser waveguide.[18] We evaluated the beam spot size of our terahertz laser in the sample plane where the beam is tightly focused using the knife-edge method.[13] A sharp metallic blade was placed in the focal plane and moved along the x (horizontal) and y (vertical) directions, perpendicular to its orientation length. The collected signal was then analyzed using the error function, $I(x) = I_0 \frac{1}{2}(1+\mathrm{erf}\{2\sqrt{\ln 2}[(x-x_c)/d]\})$, where I_0 is the full beam intensity, x is the position, x_c is the center of distribution, and d is the width at half maximum. Assuming the beam intensity profile follows a Gaussian distribution, spot sizes were determined at the full width at half maximum of the Gaussian curves. The best spot size, which determines the image resolution, was 280 μm (x) and 340 μm (y) in diameter, which is still larger than the diffraction limited spot size. Another important factor that influences the image quality is the signal to noise ratio (SNR). The noise level due to the dark current of the detector was 1 mV. This gives a dynamic range of 2000:1, which is 33 dB in our system.

In the following, we demonstrate images of various biological tissues taken using our terahertz-QC laser system. In this study, we focus on the transmission image technique, however, the reflection image modality can give similar or even better information where water absorption is crucial and forbids obtaining clear contrast. To examine the capabilities of our transmission image technique and to achieve a clear interpretation of the terahertz images, we first made a simple model of a sample containing different kinds of tissues. Freshly cut pieces from various different parts (i.e., liver, fat, muscle, and tendon) of untreated tissue were prepared and mounted on the sample holder. To ensure the exact same transmission condition is achieved, these four tissues were mounted together on the sample holder. This way, the same sample thickness was obtained by adjusting the separation between the top and bottom plates of the sample holder. A thickness of 2 mm was chosen for this study. Figure 2 shows the resulting terahertz images from these samples and a comparison with their optical images (photograph). The sample sizes were 20×3 mm^2 and the image consists of 671 pixels with a spacing of 300 μm between neighboring pixels. The total scanning time takes 30 min. Although there is a little fuzziness of each boundary, the four different sections were clearly distinguished by differences in transmitted power that come from variations in water and fat content. Liver contains more fat cells than muscle or tendon tissues, therefore liver and fat exhibit similar transmission in this measurement. Muscle and tendon contain higher water content and very little fat, therefore, exhibit muscle and tendon rather small transmission and in turn produce a very dark image. The change of contrast within the same tissue, especially muscle, is due to the inhomogeneity of the samples, which can be partly seen in the photograph. The absorption coefficients of the four different tissues were obtained at a frequency of 3.7 THz from the intensity measurement of the transmitted power of terahertz radiation. The transmitted power intensity of terahertz radiation of each tissue was determined from the average value of 100 data points in this case. Considering the difference of absorption coefficients between fat tissues (B) (which is fat+water) and others, quantitative differences in water content of each tissue were compared. The results are summarized in Table I. A and B are expected to have similar water content, and the contrast between B and C comes from $\sim$8% increase of the water content.

Next, we discuss the terahertz images of thin sections of rat brain and liver. Both rat brain and liver samples were fixed in formalin and sliced to a thickness of 2 mm. The samples were not dehydrated in alcohol, but instead air dried right before terahertz scanning, thus providing natural levels

TABLE I. Comparison of absorption coefficient differences between fat tissues (B) and others, and corresponding water content differences.

	A (liver)	C (muscle)	D (tendon)
$\Delta\alpha$	0.05	19.15	19.04
Water (%)	0.2	7.8	7.8

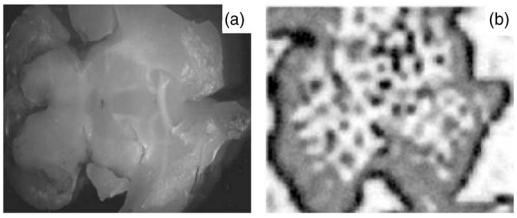

FIG. 3. Optical (white light) image (a) and terahertz image (b) of a brain slice. The sample size is $12\times10\times2$ mm^3. Terahertz image consists of 1394 pixels. For the terahertz images the lowest transmission is indicated by black and highest transmission by white.

of water content in the structures for terahertz imaging. Figure 3 shows comparison between optical image (a) and terahertz image (b) of the slice of rat brain. The sample size was 12×10 mm^2 and the terahertz image consists of 1394 pixels with 300 μm spacing between each pixel. The contrast between inner white matter and outer gray matter is clearly shown in brain image (b), where the white matter contains more fat than the outer part, which naturally has higher contents of water and proteins.

In Fig. 4, both healthy liver [(a) and (b)] and metastasis liver [(c) and (d)] slices were investigated. The sample size of the healthy liver slice is 10×8 mm^2 and the size of the metastasis liver slice is 12×7 mm^2. The terahertz images consist of 2091 pixels in (b) and 2196 pixels in (d). Both images have 200 μm spacing between each pixel. The metastasis liver sample for this experiment contains tumors developed by the research laboratory of the Department of Oncology. Terahertz image (b) shows an interesting feature in pathological term. We can observe the blood vessels in the liver at both optical image (a) and terahertz image (b), but it seems blood vessels are surrounded by more fatty tissues than the other area, which is indicated in terahertz images as white compared with the other area. In addition, terahertz image (b) is directly compared with image (d) of metastasis liver. Compared with relatively uniform transmission, which results in smooth features in the terahertz image of a healthy liver, terahertz image (d) of the metastasis liver is more complicated. The tumors are fully developed in this liver, which causes inhomogeneous tissue densities,[11,19] which the terahertz image reflects as severe fluctuation of its transmission characteristics. In addition, the tumor usually contains more water and less fat, which is resolved in terahertz imaging as darker areas. We also found the terahertz image contains comparable information to the histological sample used in pathological study. The histology sample is 5 μm thick and obtained under the treatment with chemicals. We did not fully map the information between the terahertz image and histological sample in this study, which is under investigation. However, clear relation between them indicates that terahertz image contains information in far more depth compared with optical images, and can be explained as a severe structural deformation and variation of the tissue density due to the aggressively developed tumors in liver.

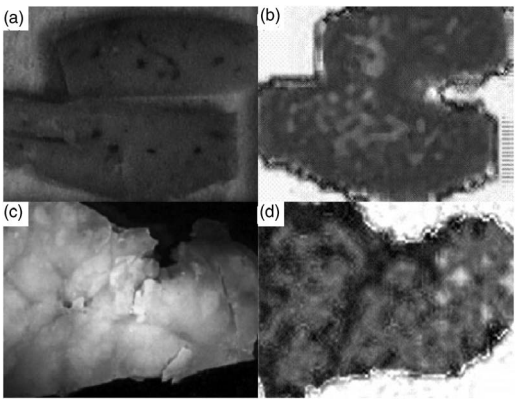

FIG. 4. Comparison between healthy liver and metastasis liver through terahertz imaging method. The sample size of the healthy liver slice [(a) and (b)] is $10\times8\times2$ mm^3 and 2091 pixels with 200 μm spacing in terahertz image (b). The sample size of the metastasis liver [(c) and (d)] is $12\times7\times2$ mm^3 and 2196 pixels in terahertz image (d). For the terahertz images the lowest transmission is indicated by black and highest transmission by white.

In summary, we built a single frequency, 3.7 THz imaging system using a quantum cascade laser. Biological tissues were studied and a small mammalian brain slice and metastasis liver tissues, were effectively probed and their structural contrast was derived from differential absorption of terahertz radiation.

The authors thank Q. Yang and D. Arvanitis for providing the tissues and M. Morf for useful discussions, and acknowledge the Beckman Institute at Stanford University for funding this research through the Ludwig Translational Cancer Research Program. One of the authors (F.H.) would like to acknowledge the Alexander von Humboldt foundation for supporting her research at Stanford University.

[1] B. B. Hu and M. C. Nuss, Opt. Lett. **20**, 1716 (1995).
[2] C. Fattinger and D. Grischkowsky, Appl. Phys. Lett. **54**, 490 (1989).
[3] D. M. Mittleman, R. H. Jacobsen, and M. C. Nuss, IEEE J. Sel. Top. Quantum Electron. **2**, 679 (1996).
[4] S. W. Smye, J. M. Chamberlain, A. J. Fitzgerald, and E. Berry, Phys. Med. Biol. **46**, R101 (2001).
[5] S. Matsuura, G. A. Blake, R. A. Wyss, J. C. Pearson, C. Kadow, A. W. Jackson, and A. C. Gossard, Appl. Phys. Lett. **74**, 2872 (1999).
[6] T. L. J. Chan, J. E. Bjarnason, A. W. M. Lee, M. A. Celis, and E. R. Brown, Appl. Phys. Lett. **85**, 2523 (2004).
[7] P. Han, G. Cho, and X.-C. Zhang, Opt. Lett. **25**, 242 (2000).
[8] D. D. Arnone, C. M. Ciesla, A. Corchia, S. Egusa, M. Pepper, J. M. Chamberlain, C. Bezant, and E. H. Linfield, Proc. SPIE **3828**, 209 (1999).
[9] E. Pickwell, B. E. Cole, A. J. Fitzgerald, M. Pepper, and V. P. Wallace, Phys. Med. Biol. **49**, 1595 (2004).
[10] R. M. Woodward, B. Cole, V. P. Wallace, R. Pye, D. D. Arnone, E. H. Linfield, and M. Pepper, Phys. Med. Biol. **47**, 3853 (2002).
[11] P. Knobloch, C. Schildknecht, T. Kleine-Ostmann, M. Koch, S. Hoffmann, E. Rehberg, M. Sperling, K. Donhuijsen, G. Hein, and K. Pierz, Phys. Med. Biol. **47**, 3875 (2002).
[12] K. J. Siebert, H. Quast, R. Leonhardt, T. Löffler, M. Thomson, T. Bauer, and H. G. Roskos, Appl. Phys. Lett. **80**, 3003 (2002).
[13] A. Dobroiu, M. Yamashita, Y. N. Ohshima, Y. Morita, C. Otani, and K. Kawase, Appl. Opt. **43**, 5637 (2004).
[14] R. Köhler, A. Tredicucci, F. Beltram, H. E. Beere, E. H. Lin-field, A. G. Davies, D. A. Ritchie, R. C. Iotti, and F. Rossi, Nature (London) **417**, 156 (2002).
[15] L. Ajili, G. Scalari, J. Faist, H. Beere, E. Linfield, D. Ritchie, and G. Davies, Appl. Phys. Lett. **85**, 3986 (2004).
[16] B. S. Williams, S. Kumar, Q. Hu, and J. L. Reno, Opt. Express **13**, 3331 (2005).
[17] J. Darmo, V. Tamosiunas, G. Fasching, J. Kröll, K. Unterrainer, M. Beck, M. Giovannini, J. Faist, C. Kremser, and P. Debbage, Opt. Express **12**, 1879 (2004).
[18] G. Scalari, N. Hoyler, M. Giovannini, and J. Faist, Appl. Phys. Lett. **86**, 181101 (2005).
[19] J. Nishizawa, T. Sasaki, K. Suto, T. Yamada, T. Tanabe, T. Tanno, T. Sawai, and Y. Miura, Opt. Commun. **244**, 469 (2005).